Available online at www.sciencedirect.com

ScienceDirect

Energy Procedia 76 (2015) 311 – 320

Energy Procedia

European Geosciences Union General Assembly 2015, EGU

Division Energy, Resources & the Environment, ERE

Numerical investigation of thermoelastic effects on fault slip tendency during injection and production of geothermal fluids

Antoine B. Jacquey[a,b,c,*], Mauro Cacace[a], Guido Blöcher[a], Magdalena Scheck-Wenderoth[a,c]

[a] *GFZ German Research Centre for Geosciences, Telegrafenberg, 14473 Potsdam, Germany*
[b] *RWTH Aachen University, Aachen Institute for Advanced Study in computational Engineering Science (AICES), Aachen, Germany*
[c] *RWTH Aachen University, Dept. of Geology, Geochemistry of Petroleum and Coal, Templergraben 55, 52056 Aachen, Germany*

Abstract

This study deals with numerical analysis of fault slip behaviour within deep faulted geothermal reservoirs during injection and production of fluid. A coupled approach for thermo-hydro-mechanical process modelling is used to describe and quantify the effects of thermoelastic stress on the slip tendency. The results show that the slip tendency of a fault can increase when the cold fluid front reaches the fault due to thermal stress enhancement. Magnitudes of increase in slip tendency depend on the injection temperature and the dip angle of the fault, and under specific configurations, may lead to a reactivation of the fault.

Peer-review under responsibility of the GFZ German Research Centre for Geosciences

Keywords: Slip tendency, Thermoelasticity, Enhanced geothermal systems

1. Introduction

Understanding processes controlling slip behaviour of faults as induced by man-made activities is of interest for several geo-energy related studies such as geothermal power production, energy storage and enhanced oil and gas recovery. Injection-induced reactivation of faults or fracturing can indeed lead to notable micro-earthquakes [1,2,3,4]. Correlations between pore pressure changes as those induced by injection and production of fluid and the in-situ stress field within a reservoir play a major role in coupled hydraulic and deformation processes [5,6,7]. These poroelastic effects have been identified as part of the processes controlling faults slip behaviour [8,9,3,4]. Furthermore, changes in temperature can also affect the in-situ stress-field [10,11,12,13]. Although the ratio between thermoelastic and poroelastic stresses ($\sigma^{Thermo}/\sigma^{Poro} = K\beta\Delta T/\alpha\Delta p_f$) has been reported to increase with rock stiffness and therefore depth [14], thermoelastic effects are often not considered when analysing slip tendency and possible reactivation of faults in geothermal reservoirs.

* Corresponding author. Tel.: +49-331-288-1779 ; fax: +49-331-288-1349.
E-mail address: antoine.jacquey@gfz-potsdam.de

Peer-review under responsibility of the GFZ German Research Centre for Geosciences
doi:10.1016/j.egypro.2015.07.868

Nomenclature

$c_{f,s,b}$	fluid, solid or bulk heat capacity
E	Young's modulus
$\boldsymbol{g}$	gravitational force
G	shear modulus
$\boldsymbol{I}$	identity matrix
$\boldsymbol{k}$	permeability tensor
K	bulk modulus
L	first Lamé parameter
$n_{x,y,z}$	direction cosines
p_f	pore pressure field
$\boldsymbol{q_f}$	specific discharge or Darcy's velocity
$Q_{f,T}$	fluid (subscript f) or thermal (subscript T) source term
S_s	specific storage
t	time
T	temperature field
T_0	initial temperature
T_s	slip tendency
$\boldsymbol{v_f}$	fluid velocity
α	Biot's elastic coefficient
β	thermal expansion coefficient
γ	dip angle
δ_{ij}	Kronecker-delta
$\boldsymbol{\epsilon}$	strain tensor
$\lambda_{b,s}$	bulk or solid thermal conductivity
μ_f	fluid dynamic viscosity
μ_s	solid frictional coefficient
ν	Poisson's ratio
$\rho_{f,s,b}$	fluid, solid or bulk density
$\boldsymbol{\sigma}$	Cauchy's stress tensor
$\boldsymbol{\sigma'}$	effective stress tensor
σ_N	normal stress
τ	shear stress
$\mathbb{C}$	elastic material tensor

This contribution presents a numerical evaluation of the impacts of thermoelastic stresses on the slip behaviour of faults within deep geothermal reservoirs as based on a frictional sliding resistance formulation. A coupled approach for thermo-hydro-mechanical process modelling has been integrated in the open-source finite element method based simulator OpenGeoSys [15] following theory of coupled thermo- and poroelasticity.

The reactivation potential of a fault is evaluated during injection and production of geothermal fluid as a function of the ratio of shear to normal stress on the fault plane. First, a simple geometry model is considered with different configurations, by changing the dip angle of the fault. Thermoelastic stress enhancement comes from the temperature anomaly of the cold injected geothermal fluid propagating within the relative warmer fluid-bearing reservoir. This simple model serves as an introduction to a real-case application of the Groß Schönebeck geothermal research site, which is discuss further in the manuscript.

2. Approach

2.1. Governing equations for thermo-hydro-mechanical process modelling

Governing equations for fluid-flow, heat transport and elastic deformation as required to solve coupled thermo-hydro-mechanical (THM) processes are derived from balance equations of mass, heat and momentum. In this section, the governing equations as they are implemented in OpenGeoSys [15] are presented.

Governing equation for fluid flow results from conservation of mass in a fully saturated porous medium:

$$\frac{S_s}{\rho_f g}\frac{\partial p_f}{\partial t} + \nabla \boldsymbol{q_f} = Q_f \tag{1}$$

The discharge $\boldsymbol{q_f}$ can be expressed via the Darcys law resulting from conservation of momentum:

$$\boldsymbol{q_f} = -\frac{\boldsymbol{k}}{\mu_f}\left(\nabla p_f - \rho_f \boldsymbol{g}\right) \tag{2}$$

Heat transport governing equation is derived from heat balance considering conductive and advective heat transport processes. Thermal equilibrium between fluid and solid is assumed.

$$(\rho c)_b \frac{\partial T}{\partial t} + \phi\,(\rho c)_f \boldsymbol{v_f} \nabla T - \nabla.\,(\lambda_b \nabla T) = Q_T \tag{3}$$

The product ρc is often called the heat storage. Subscript b refers to the bulk, subscript s to the solid phase and subscript f to the fluid phase. The relation between the heat storage of each phase (mean algebraic mixing rule) is: $(\rho c)_b = \phi\,(\rho c)_f + (1-\phi)\,(\rho c)_s$.

Deformation of the porous medium in a context of poro-and thermoelasticity [12,13] is governed by the momentum balance equation in terms of stress:

$$\nabla.\left(\boldsymbol{\sigma'} - \alpha p_f \boldsymbol{I} - K\beta\,(T - T_0)\,\boldsymbol{I}\right) + \rho_s \boldsymbol{g} = 0 \tag{4}$$

Where $\boldsymbol{\sigma'}$ is the effective stress tensor defined after [6]:

$$\boldsymbol{\sigma'} = \boldsymbol{\sigma} + \alpha p_f \boldsymbol{I} \tag{5}$$

With $\boldsymbol{\sigma}$ the total Cauchy's stress tensor. Effective stress tensor is related to strain via the generalized Hooke's law extended for non-isothermal deformation:

$$\Delta\boldsymbol{\sigma'} = \mathbb{C}\left(\Delta\boldsymbol{\epsilon} - \frac{1}{3}\beta\Delta T\boldsymbol{I}\right) \tag{6}$$

Where $\mathbb{C}$ is the elastic material tensor, expressed as:

$$\mathbb{C} = L\delta_{ij}\delta_{kl} + 2G\delta_{ik}\delta_{jl} \tag{7}$$

Inverting Eq. 6 leads to the strains:

$$\epsilon_{xx} = \frac{1}{E}\left(\sigma'_{xx} - \nu(\sigma'_{yy} + \sigma'_{zz})\right) + \frac{1}{3}\beta\Delta T \tag{8}$$

$$\epsilon_{yy} = \frac{1}{E}\left(\sigma'_{yy} - \nu(\sigma'_{xx} + \sigma'_{zz})\right) + \frac{1}{3}\beta\Delta T \tag{9}$$

$$\epsilon_{zz} = \frac{1}{E}\left(\sigma'_{zz} - \nu(\sigma'_{xx} + \sigma'_{yy})\right) + \frac{1}{3}\beta\Delta T \tag{10}$$

It is worth noticing that the approach presented here does not describe undrained effects such as mechanical and thermal pressurization (increase of pore pressure due to stress and temperature changes).

2.2. Slip tendency

Slip tendency is the ratio of resolved shear stress to normal stress acting on the fault plane [16,17]. If the shear stress exceeds the frictional sliding resistance (here parametrized in terms of a sliding coefficient μ_s after [18]), slip is likely to occur on the fault plane, which can be described as:

$$T_s = \frac{\tau}{\sigma'_N} \leq \mu_s \tag{11}$$

Here, it is assumed a sliding coefficient μ_s of 0.85 which better defines shear failure at shallow crustal depth (from 1 to 5 km) [18]. Eq. 11 is only valid for normal stress smaller than 200 MPa [8]. Orientation of the plane can be defined by means of the three angles between the planes normal and each of the principal stress axes. In all simulations presented, principle stress axes match coordinate axes. The direction cosines of these angles (n_x, n_y and n_z) are related with the following relation (Pythagoras theorem):

$$n_x^2 + n_y^2 + n_z^2 = 1 \tag{12}$$

Shear and normal stresses acting on a plane the orientation of which is defined by the three previous direction cosines can be calculated after [19,8,1] as:

$$\sigma'_N = n_x^2\sigma'_{xx} + n_y^2\sigma'_{yy} + n_z^2\sigma'_{zz} \tag{13}$$

$$\tau = \sqrt{n_x^2 n_y^2 \left(\sigma_{xx} - \sigma_{yy}\right)^2 + n_y^2 n_z^2 \left(\sigma_{yy} - \sigma_{zz}\right)^2 + n_x^2 n_z^2 \left(\sigma_{xx} - \sigma_{zz}\right)^2} \tag{14}$$

2.3. Model setup

The approach presented in the previous sections is applied on a simple geometry model. The model consists of a homogeneous reservoir (target depth 4000 meters below sea level) with a fault discretized in 3 dimensions (20 meters width) with a dip angle noted γ ($\gamma = \pi/4 = 45°$). Two hydraulically induced fractures from each side of the fault are integrated in the model where injection and production of the geofluid occur. The model is 1 km large in horizontal direction and 200 m high in vertical direction. The geometry of this model is schematically illustrated in Fig. 1.

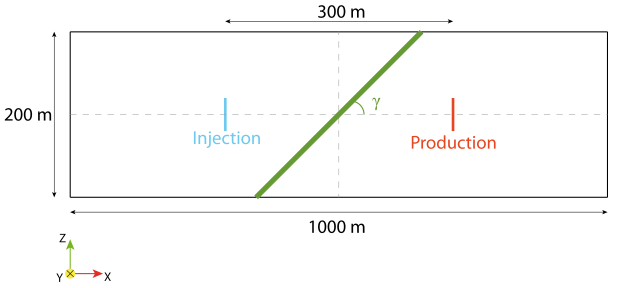

Fig. 1. Geometry of the 3-dimensional model used for the simulations. Here, a vertical cross-section is shown for a constant plane at $Y = 0$. Model is 1 km large in horizontal direction (X and Y directions) and 200 meters height in vertical direction (Z). The geometry of the fault plane (in green) is characterized by its dip angle (γ). Injection and production fractures (in blue and red respectively) are orthogonal to the X direction and are 100 meters large squares. Distance between the injection and the production fractures is 300 meters.

Geometrical discretization of the model has been done using an in house open-source meshing software MeshIt [20], allowing the transfer of the geometrical configuration of the model to the Finite-Element solver. A normal faulting stress regime is considered ($\sigma_1 = \sigma_{zz}$, $\sigma_2 = \sigma_{yy}$ and $\sigma_3 = \sigma_{xx}$) characterized by the following stress magnitudes:

- $\sigma_1 = -95$ MPa

- $\sigma_2 = -75$ MPa
- $\sigma_3 = -70$ MPa

Initial conditions for pore pressure, temperature and stress distributions are obtained from a steady-state simulation, for which a hydrostatic distribution of pore pressure (43.5 MPa at 4 km depth) and a geothermal gradient of ($33°C\,km^{-1}$) are assumed (Fig. 2).

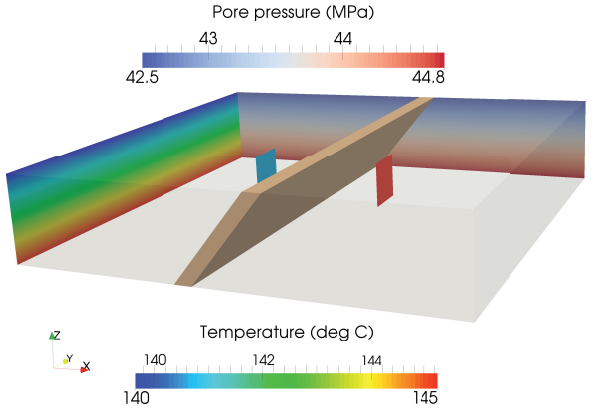

Fig. 2. Initial pore pressure and temperature distributions within the reservoir.

Water is injected with a temperature of 70°C at 75 $m^3\,h^{-1}$ at the injection fracture (in blue in Fig. 1 and 2). Symmetrically, 75 $m^3\,h^{-1}$ of warm water (in-situ temperature) is produced at the production fracture (in red in Fig. 1 and 2). Physical properties of the reservoir and the fault are listed in Table 1.

Table 1. Properties of the homogeneous reservoir and the fault (density ρ, porosity ϕ, permeability k, solid thermal capacity c_s, solid thermal conductivity λ_s, thermal expansion coefficient β, bulk modulus K, solid bulk modulus K_s and Poisson's ratio ν).

	ρ [kg m^{-3}]	ϕ [%]	k [m^2]	c_s [W kg^{-1} K^{-1}]	λ_s [W m^{-1} K^{-1}]	β [K^{-1}]	K [GPa]	K_s [GPa]	ν [-]
Reservoir	2650	12.5	1.28×10^{-14}	920	3.1	1.0×10^{-5}	60	70	0.31
Fault	2650	43	1.28×10^{-14}	1000	3.0	1.0×10^{-5}	20	41.5	0.1

3. Results

3.1. Initial slip tendency

Initial slip tendency can be evaluated using Eq. 11, 12, 13 and 14 and as a function of the dip angle γ. Analytically, the initial slip tendency is evaluated as 0.28. However, this value is obtained by assuming a homogeneous stress distribution within the reservoir, conditions that are not met within the model domain which is characterized by a fault having different mechanical properties than the hosting reservoir (Table 1). Initial mean effective stress distribution (negative for compression) and vertical displacement computed from the steady-state simulation are illustrated on Fig.3. Highest values of the mean effective stress are localized at the interface between the fault and the reservoir while lowest values are within the fault, where also the lowest values for the vertical displacement localize.

Under the given stress distribution as initial condition, the slip tendency is calculated to be in average 0.3. This higher value than the analytical one comes from stress localization at the reservoir/fault interface. The fault acts as a heterogeneity in terms of mechanical properties. This leads to build up of stresses along the contact surface area with the reservoir thus explaining the higher slip tendency observed within this domain.

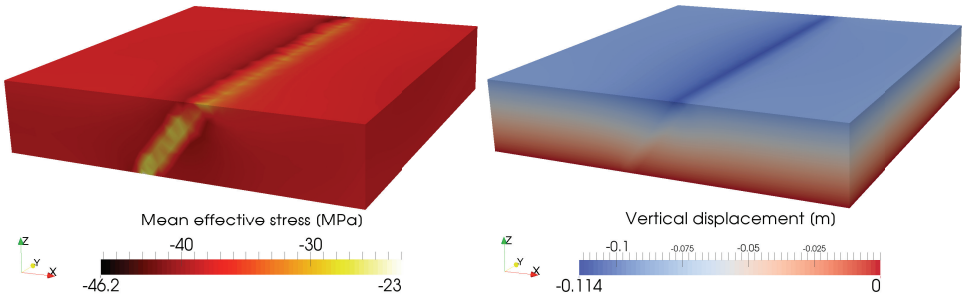

(a) (b)

Fig. 3. Initial mean effective stress distribution (a) and vertical displacement (b) computed from the steady-state simulation using the regional stress field. Negative effective stress relates compressive regime

3.2. Dynamic evolution of slip tendency

Injection of cold fluid induce poroelastic and thermoelastic stresses within the reservoir. Unlike the temperature distribution which is governed by conduction and advection (Eq. 3), the pressure distribution is only governed by diffusion (Eq.1 and 2). Therefore pore pressure changes are mostly localized at the injection and production fractures. No significant pore pressure changes are noticeable on the fault plane. Only thermoelastic stress changes have therefore an impact on the slip behaviour of the fault.

When the cold water front reaches the fault, normal and shear stress acting on the fault plane are enhanced by thermal effects. In this section, dynamic evolution of the slip tendency is analysed, as a function of temperatures changes modelled during geothermal operations.

Fig. 4 shows the obtained results after 15 years of injection, including the 3-D model and the 130°C isotherm reaching the fault (Fig. 4.a), the slip tendency T_s on the fault plane (Fig. 4.b), the temperature difference dT from the initial state (Fig. 4.c) and the slip tendency difference dT_s from the initial state (Fig. 4.d).

As seen on Fig. 4(c) and Fig. 4(d), a 30°C decrease in temperature lead to an increase of about 0.6 in slip tendency due to a thermally induced increase in shear stress and decrease in normal stress. This results in a total slip tendency reaching almost 1 at the hitting point of the cold fluid. Assuming a frictional coefficient of $\mu_s = 0.85$ [18], it follows from Eq. 11 that under these conditions the fault is likely to be reactivated. However, this high slip value is localized and not homogeneously distributed within the entire fault plane.

It is worth noticing that the small increase of slip tendency (+0.2 in light blue) localized in the upper part of the fault is due to poroelastic effects. Indeed, a slight pore pressure increase (+0.1 MPa) is predicted at this location on the fault plane.

3.3. Influence of the fault dip angle

Changing the dip angle of the fault influences the initial slip tendency, as well as its dynamic evolution. Under a normal faulting regime as specified in the previous section, decreasing the dip angle of the fault decreases the slip tendency ($\sigma_1 = \sigma_{zz}$).

To quantify these effects, two additional scenarios are investigated as shown in Fig. 4. These two scenarios corresponds to two different values of the dip angle of the fault γ (see Fig. 5.):

- Reference dip angle: $\gamma = \pi/4 = 45°$ (results presented on Fig. 4).
- Low dip angle: $\gamma = \pi/8 = 22.5°$.
- High dip angle: $\gamma = 3\pi/8 = 67.5°$.

Calculated initial slip tendency is 0.2 for the low dip angle case (Fig. 5(a)) and 0.4 for the high dip angle case (Fig. 5(b)). After 15 years of injection, these two additional fault configurations give interesting insights on the

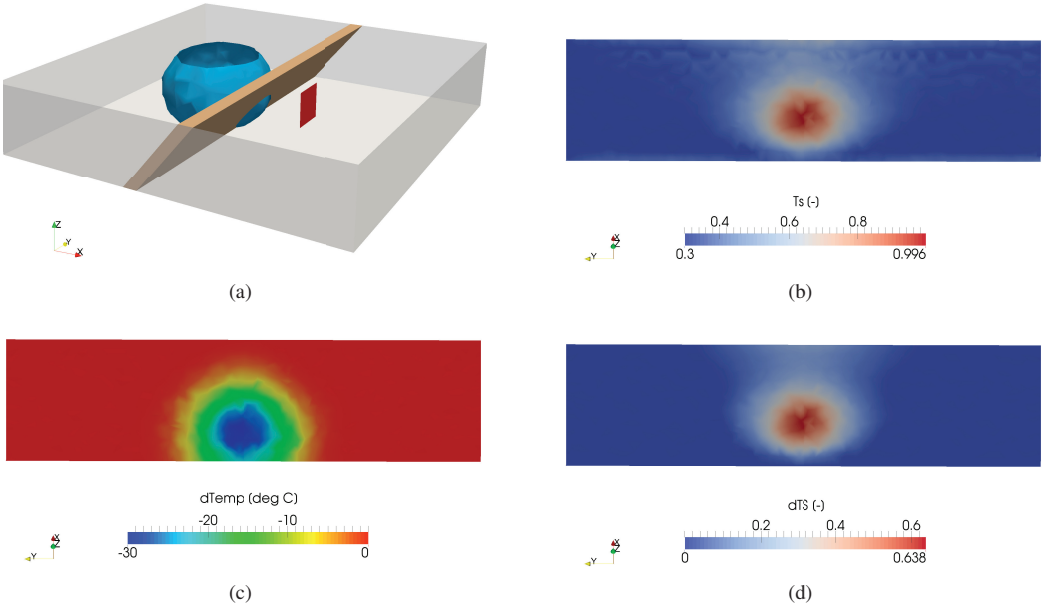

Fig. 4. Results after 15 years of injection. (a) The 3-D model with the 130°C isotherm (in blue). (b) 2-D view of a cross-section on the fault place showing the slip tendency distribution. (c) On the same cross-section, distribution of the temperature difference with initial conditions. (d) On the same cross-section, distribution of the slip tendency difference with initial conditions.

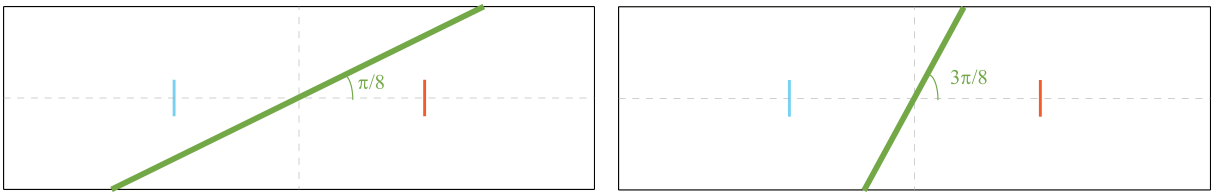

(a) Low dip angle case (b) High dip angle case

Fig. 5. Two additional scenarios in terms of dip angle of the fault. (a) Low dip angle model with $\gamma = \pi 8$. (b) High dip angle model with $\gamma = 3\pi 8$.

thermoelastic response of the slip tendency. For the low dip angle case, a 60°C decrease in temperature is observable on the fault plane with a similar distribution as for the reference case (see Fig. 4(c)). However the observed 60°C decrease in temperature leads to a +0.3 increase in slip tendency. Furthermore, for the high dip angle case, a 20°C decrease in temperature leads to a +1 increase in slip tendency. These results are summarized in Fig. 6. Differences in the temperature distribution for the two cases result from differences in the geometry of the model. As seen on Fig. 5, if the dip angle is lowered, the cold water front will hit the fault at earlier stages and coldest temperatures will be observed in the lower part of the fault.

For a given in-situ stress field (here normal faulting), the dip angle of the fault has a significant influence on the increase in slip tendency resulting from thermoelastic effects (from +0.3 to +1 increase in slip tendency).

4. Discussion: real-case application of the Groß Schönebeck geothermal reservoir

The approach presented in this contribution has been applied on a real-case application: the geothermal research site of Groß Schönebeck (40 km north of Berlin, Germany). This site consists in a geothermal doublet (target depth of −4100 m) drilled with a faulted reservoir. Geological context of this reservoir, stimulation treatments as well as dynamic modelling of thermo-hydraulic processes are well described in the literature [21,1,22,23,24]. An approach for coupled thermo-hydro-mechanical processes similar to the one presented in section 2 with transport properties

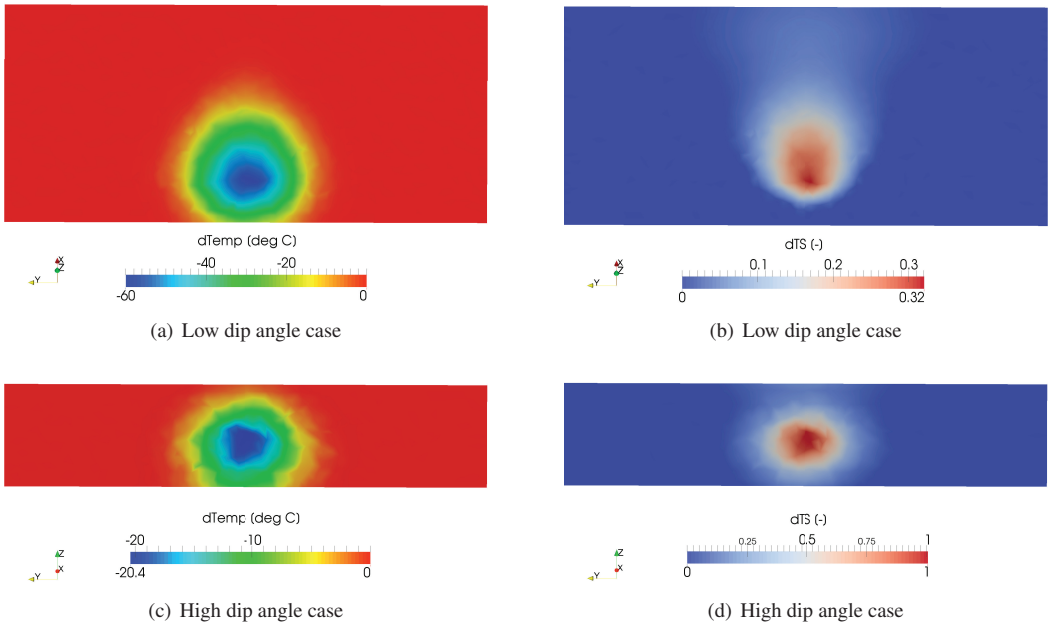

(a) Low dip angle case (b) Low dip angle case

(c) High dip angle case (d) High dip angle case

Fig. 6. Results after 15 years of injection. (a) Distribution of the temperature difference with initial conditions on the fault plane for the low dip angle case. (b) Distribution of the slip tendency difference with initial conditions on the fault plane for the low dip angle case. (c) Distribution of the temperature difference with initial conditions on the fault plane for the high dip angle case. (d) Distribution of the slip tendency difference with initial conditions on the fault plane for the high dip angle case.

evolution models has been applied to a 3-dimensional discretized model of the Groß Schönebeck reservoir [20]. 70°C fluid is injected in the reservoir with a rate of 30 $m^3\,h^{-1}$. The in-situ temperature within the reservoir ranges from 145 to 150°C. The in-situ stress-field is transitional regime between normal faulting and strike-slip faulting [21].

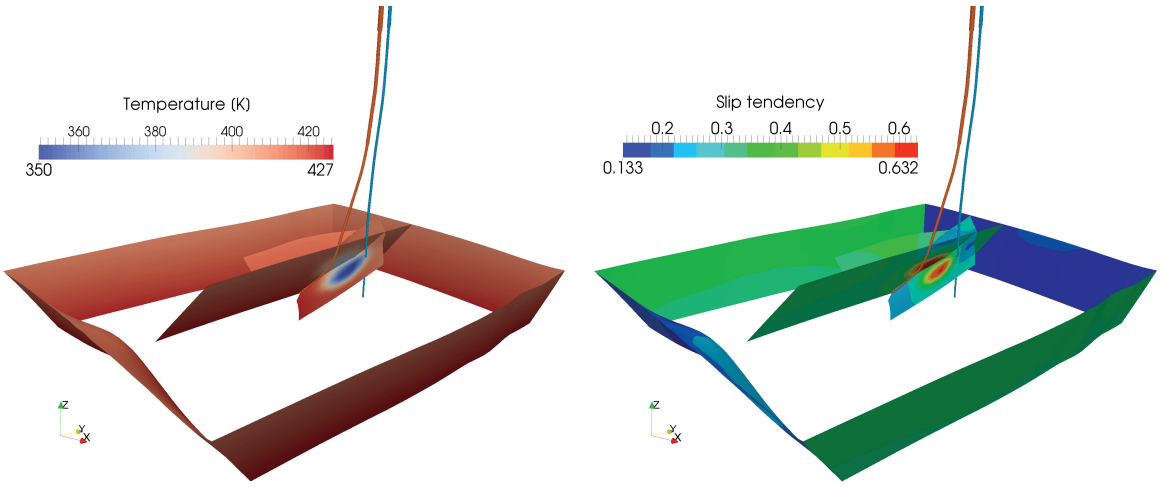

(a) (b)

Fig. 7. Results of fully coupled THM process modelling for the Groß Schönebeck geothermal reservoir. Here only the faults in the reservoir are shown after 100 years of injection of cold fluid (70°C) at 30 $m^3\,h^{-1}$. (a) Temperature distribution. (b) Slip tendency. The blue line represent the path of the injection well and the red one the path of the production well.

Fig. 7 shows the temperature distribution (Fig. 7(a)) and the slip tendency (Fig 7(b)) distribution along the major faults within the reservoir after 100 years of simulated operation time. A temperature decrease of about 70°C leads to an increase in slip tendency of about +0.6 on two different faults. This increase in slip tendency is localized on the faults around the injection well (blue line on Fig. 7) as well behind the production well (red line on Fig. 7). The magnitude of slip tendency could lead to alteration of the slip behaviour of the fault and in extreme case, to reactivation of the fault (if $T_s \geq \mu_s$) and therefore to the generation of seismic events. Microseismicity activity has been recorded during water frac treatment of the production well drilled in 2007 [25]. These microseismic events have been related to pressure diffusion effects (rapid injection of fluid) and have shown that the faults around the well have a high reactivation potential. The present study supports the idea that these faults are initially critically stressed (in accordance with [1]) and that they also present high reactivation potential, here caused by thermal stress enhancement. However, whether such a dynamic relation between these processes exists and what implications it imports in terms of reservoir sustainability remains only speculative at this stage.

As reported by several studies, formulations of the theory of thermoelasticity show strong similarities to formulations adopted to describe poroelastic phenomena [10,11,12,13]. Where an effective stress law has been introduced in the theory of poroelasticity [5,6] to correct the effect of pore pressure on deformation, the results presented in the present study suggest the need of an extended effective stress law correcting also for temperature changes effects, taking the form:

$$\boldsymbol{\sigma}' = \boldsymbol{\sigma} + \alpha p_f \boldsymbol{I} + K\beta (T - T_0) \boldsymbol{I} \tag{15}$$

This new formulation for the effective stress tensor would also induce an increase in normal stress acting on the fault plane (Eq. 13) which could contribute to correct the increase of slip tendency due to temperature decrease. Validation of the new formulation is part of ongoing work.

In this approach, a one way coupling for thermo-mechanical processes has been discussed, that is, the temperature distribution has an impact on the deformation (thermal strain and stress) but deformation has no influence on the temperature field. This assumption, though valid in most materials may not be considered realistic for coupled thermo-hydro-mechanical processes modelling in such applications. Indeed, in the case of faulted reservoir, processes such as shear heating can occur and influence the temperature distribution along a fault plane. This contribution therefore raises the need of a stronger coupling between thermal, hydraulic and mechanical processes taking into account all dynamic feedbacks to better describe changes in the in-situ stress field acting on faults which are of relevance for the studying of their potential reactivation during man-made activities.

5. Conclusion

For deep geothermal reservoirs, thermoelastic stress often exceeds poroelastic stress (by a factor of 10 for the given configuration). Changes in temperature induced by injection of cold fluid control therefore the in-situ stress field. Such phenomenon has a direct impact on slip tendency of major fault zones. In the present study, it has been shown that injection temperature and geometry of the fault (dip angle) play an important role in evaluating the fault reactivation potential. In general, slip is more likely to occur when the cold fluid front hit the fault plane. Similar conclusions have been derived for a real-case study based on the geothermal facility of Groß Schönebeck. These preliminary studies elucidate the importance of thermal effects on the mechanical stability of major fault zones during geothermal reservoir activities and raises the importance of deepening the coupling among thermo-hydro-mechanical processes affecting the reservoir.

Acknowledgements

This work has been performed in the framework of the project Portfolio - Geoenergy funded by the Helmholtz Association.

References

[1] Moeck, I., Kwiatek, G., Zimmermann, G.. Slip tendency analysis, fault reactivation potential and induced seismicity in a deep geothermal reservoir. J Struct Geol 2009;31:1174–1182.

[2] Deichmann, N., Giardini, D.. Earthquakes Induced by the Stimulation of an Enhanced Geothermal System below Basel (Switzerland). Seismol Res Lett 2009;80:784–798.

[3] Rutqvist, J., Rinaldi, A.P., Cappa, F., Moridis, G.J.. Modeling of fault reactivation and induced seismicity during hydraulic fracturing of shale-gas reservoirs. J Pet Sci Eng 2013;107:31–44.

[4] Rutqvist, J., Rinaldi, A.P., Cappa, F., Moridis, G.J.. Modeling of fault activation and seismicity by injection directly into a fault zone associated with hydraulic fracturing of shale-gas reservoirs. J Pet Sci Eng 2015;127:377–386.

[5] Terzaghi, K.. Theoritical Soil Mechanics. John Wiley & Sons; 1943.

[6] Carrol, M.M., Katsube, N.. The Role of Terzaghi Effective Stress in Linearly Elastic Deformation. J Energy Ressources Technol 1983;.

[7] Soltanzadeh, H., Hawkes, C.D., Smith, S.A.. Poroelastic Modelling of Production and Injection-Induced Stress Changes in a Pinnacle Reef. In: Proc. RockEng09, Rock Eng. Difficult Cond. Toronto; 2009, p. 1–12.

[8] Jaeger, J., Cook, N.G., Zimmerman, R.. Fundamentals of Rock Mechanics. Oxford: Blackwell; 2007.

[9] Cappa, F., Rutqvist, J.. Modeling of coupled deformation and permeability evolution during fault reactivation induced by deep underground injection of CO2. Int J Greenh Gas Control 2011;5:336–346.

[10] Geertsma, J.. A remark on the analogy between thermoelasticity and the elasticity of saturated porous media. J Mech Phys Solids 1957;6:13–16.

[11] Lord, H., Shulman, Y.. A generalized dynamical theory of thermoelasticity. J Mech Phys Solids 1967;15:299–309.

[12] McTigue, D.F.. Thermoelastic response of fluid-saturated porous rock. J Geophys Res 1986;91:9533.

[13] Zimmerman, R.. Coupling in poroelasticity and thermoelasticity. Int J Rock Mech Min Sci 2000;37:79–87.

[14] Segall, P., Fitzgerald, S.D.. A note on induced stress changes in hydrocarbon and geothermal reservoirs. Tectonophysics 1998;289:117–128.

[15] Kolditz, O., Bauer, S., Bilke, L., Böttcher, N., Delfs, J.O., Fischer, T., et al. OpenGeoSys: an open-source initiative for numerical simulation of thermo-hydro-mechanical/chemical (THM/C) processes in porous media. Environ Earth Sci 2012;67:589–599.

[16] Morris, A., Ferrill, D.a., Henderson, D.B.. Slip-tendency analysis and fault reactivation Slip-tendency analysis and fault reactivation. Geology 1996;24:275–278.

[17] Lisle, R.J., Srivastava, D.C.. Test of the frictional reactivation theory for faults and validity of fault-slip analysis. Geology 2004;32:569–572.

[18] Byerlee, J.. Friction of rocks. Pure Appl Geophys PAGEOPH 1978;116:615–626.

[19] Ramsay, J.G., Lisle, R.L.. Volume 3: Applications of continuum mechanics in structural geology. In: Tech. Mod. Struct. Geol. London: Academic Press; 2000, p. 560.

[20] Cacace, M., Blöcher, G.. MeshIt - a software for three dimensional volumetric meshing of complex faulted reservoirs. Environ Earth Sci 2015;.

[21] Moeck, I., Schandelmeier, H., Holl, H.G.. The stress regime in a Rotliegend reservoir of the Northeast German Basin. Int J Earth Sci 2009;98:1643–1654.

[22] Zimmermann, G., Reinicke, A.. Hydraulic stimulation of a deep sandstone reservoir to develop an Enhanced Geothermal System: Laboratory and field experiments. Geothermics 2010;39:70–77.

[23] Blöcher, G., Zimmermann, G., Moeck, I., Brandt, W., Hassanzadegan, A., Magri, F.. 3D numerical modeling of hydrothermal processes during the lifetime of a deep geothermal reservoir. Geofluids 2010;10:406–421.

[24] Blöcher, G., Zimmermann, G., Moeck, I., Huenges, E.. GroßSchönebeck (D) - Moving forward on the learning curve: lessons learned from projects in the recent years from projects. In: Int. Conf. Enhanc. Geotherm. Syst. Freiburg, Germany; 2012,.

[25] Kwiatek, G., Bohnhoff, M., Dresen, G., Schulze, A., Schulte, T., Zimmermann, G., et al. Microseismicity induced during fluid-injection: A case study from the geothermal site at GroßSchönebeck, North German Basin. Acta Geophys 2010;58:995–1020.